On the Laplace-Beltrami Operator and Brain Surface Flattening

Sigurd Angenent
Department of Mathematics
University of Wisconsin
Madison, Wisconsin 53705

Steven Haker
Department of Mathematics
University of Minnesota
Minneapolis, MN 55455

Allen Tannenbaum
Department of Electrical and Computer Engineering
University of Minnesota
Minneapolis, MN 55455
email: tannenba@ece.umn.edu
fax: 612-625-4583

Ron Kikinis
Harvard Medical School
Brigham and Women's Hospital
Harvard University
Boston, MA 02115

January 20, 2000

This work was supported in part by grants from the National Science Foundation DMS-9058492, ECS-9700588, NSF-LIS, by the Air Force Office of Scientific Research AF/F49620-98-1-0168, by the Army Research Office DAAG55-98-1-0169, and MURI Grant. All correspondence concerning this paper should be sent to Allen Tannenbaum.

Abstract

In this paper, using certain conformal mappings from uniformization theory, we give an explicit method for flattening the brain surface in a way which preserves angles. From a triangulated surface representation of the cortex, we indicate how the procedure may be implemented using finite elements. Further, we show how the geometry of the brain surface may be studied using this approach.

Keywords: Brain flattening, functional MRI, harmonic maps, segmentation.

This paper has appeared in *IEEE Transactions of Medical Imaging.*

1 Introduction

Recently a number of techniques have been proposed to obtain a flattened representation of the cortical surface; see, e.g., [6, 7, 8, 16, 28] and the references therein. Flattening the brain surface has uses in many areas including functional magnetic resonance imaging. Indeed, since it is important to visualize functional magnetic resonance imaging data for neural activity within the three dimensional folds of the brain, flattened representations have become an increasing important approach to such visualization techniques.

Our approach to flattening such a surface is based on the exploitation of a certain fact from the theory of Riemann surfaces from complex analysis and geometry, namely, that a surface of genus zero (no handles) without any holes or self-intersections can be mapped conformally onto the sphere, and any local portion thereof onto a disc. In this way, the brain surface may be flattened. The mapping is conformal in the sense that angles are preserved. It is also bijective (onto and one-to-one) and thus there is no problem with triangles "flipping" or overlapping, and no cuts need be made on the surface.

Moreover, one can explicitly write down how the metric is transformed and thus areas and the geodesics as well. Specifically, the elements of the first fundamental form (E, F, G) are transformed as $(\rho E, \rho F, \rho G)$ with ρ depending on the point of the surface. (See [9, 10] for all the details.) For this reason, conformal mappings are often described as being "similarities in the small". In short, the mapping can be used to obtain an atlas of the brain surface in a straightforward, canonical manner.

We should note that our approach is quite different from the previous works cited above in brain flattening which typically consider locally area or length preserving deformations. For example, in the nice approaches of [7, 16], the authors fit a parameterized deformable surface whose topology is mappable to a sphere. Then, it is possible to represent the brain surface on a planar map by using spherical coordinates. Work has also been done on quasi-isometries and quasi-conformal flattenings of the brain surface (see e.g., [24, 4]). In these interesting approaches, the authors start from a triangulated representation of the given surface, and typically employ a relaxation method to discretely minimize an energy functional. Thus they cannot guarantee bijectivity, and in particular cannot guarantee that triangles do not flip. In our case, our initial intuition is continuous, i.e., we explicitly construct the bijective conformal equivalence on a continuous model of the surface, and only then move to the discrete implementation. If a quasi-length or area-preserving mapping is desired, then our conformal mapping technique is a good starting point, since it efficiently *unfolds* the surface while locally preserving shape.

In our work, the key observation is that the flattening function may be obtained as the solution of a second order elliptic partial differential equation (PDE) on the surface to be flattened. For triangulated surfaces, there exist powerful, reliable finite element procedures which can be employed to numerically approximate the flattening function. Preliminary results along these lines were reported in the technical report [1]. In our case, we may use the fast segmentation methods of [15, 25, 26] to represent the cortical surface as a triangulated surface to which we apply our procedure.

The outline of this paper is as follows. In Section 2, we sketch the analytical procedure to find the flattening map, leaving most of the details for the Appendix of Section 8. In Sections 3 and 4, we describe how the numerical algorithm works on a triangulated surface. This is based on the finite element method with some key modifications to incorporate the special boundary conditions of our problem. In Section 5, we briefly review the theory of curvature flows and their use in segmentation. In Section 6, we demonstrate our procedure using real brain data, and in Section 7 we make some conclusions and discuss further research.

2 Uniformization of the Brain Surface

In this section, we sketch the mathematical justification of our brain flattening procedure. See the Appendix of Section 8 for more details. We start with the basic assumption that the brain surface may be approximated as a topological sphere. While this is is not exactly correct (there are some small holes where the ventricles connect to the outer surface), we can always fill these in by using, e.g., morphological dilation and erosion. This will not affect the structures in which we are interested in flattening, in particular the brain hemispheres. Let $\Sigma \subset \mathbf{R}^3$ represent this brain model which we assume is an embedded surface (no self-intersections) of genus 0. In this section, since we will be giving the analytical solution to the uniformization problem, we assume that Σ is a smooth manifold. For the finite element method described in the next section, it will be enough to take it as a triangulated surface. (We refer the reader to [11] for the basic theory of uniformization of Riemann surfaces, and to [22] for the solutions of elliptic PDE's and the Dirichlet problem.) Fix a point p on this surface. Let δ_p denote the Dirac delta (impulse) function at p, Δ the Laplace-Beltrami operator on $\Sigma \backslash \{p\}$, and i the square root of -1. The Laplace-Beltrami operator is the generalization of the usual Laplacian operator to a smooth surface. Let S^2 denote the unit sphere in $\mathbf{R}^3$ and let $\mathbf{C}$ be the complex plane.

Recall from the Introduction that a conformal equivalence is a one-to-one, onto mapping which preserves angles. We can now state the following result which provides the analytical basis for our texture mapping procedure:

A conformal equivalence $z : \Sigma \backslash \{p\} \to S^2 \backslash \{\text{north pole}\}$ may be obtained by solving the equation

$$\Delta z = \left(\frac{\partial}{\partial u} - i \frac{\partial}{\partial v} \right) \delta_p. \tag{1}$$

Here, u and v are conformal coordinates defined in a neighborhood of p. The definition of conformal coordinates and the derivation of this equation may be found in the Appendix of Section 8. Further, we are identifying $S^2\backslash\{\text{north pole}\}$ with the complex plane in the standard way from complex analysis, say via stereographic projection. (This is the mapping that sends (x, y, z) on the unit sphere to the point $(\frac{x}{1-z}, \frac{y}{1-z})$ in the complex plane.) This result means that we can get the conformal equivalence by solving a second order partial differential equation on the surface. Fortunately, on a triangulated surface, this may be carried out using a finite element technique we will describe below.

Remark: The map z is unique up to complex multiplication and translation, that is, any other conformal $z_1 : \Sigma\backslash\{p\} \to \mathbf{C}$ is given by $z_1 = Az + B$ for some constants $A, B \in \mathbf{C}$.

3 Finite Element Approximation of Conformal Mapping

In the previous section, we have outlined the analytical procedure for flattening the brain surface via uniformization. We want now to describe a numerical procedure for carrying this out, i.e. for solving (1). We now assume that Σ is a triangulated surface. Using the notation of the previous section, let $\sigma = ABC$ be the triangle in whose interior the point p lies.

3.1 Approximation of $\left(\frac{\partial}{\partial u} - i\frac{\partial}{\partial v}\right)\delta_p$

Equation (1) is derived in the Appendix under the assumption that we are working with smooth functions on smooth manifolds. However, in our implementation we will be working instead with a triangulated surface and an approximating space of functions. In order to solve (1), we therefore need to find an approximation to its right-hand side. The key is to interpret $\left(\frac{\partial}{\partial u} - i\frac{\partial}{\partial v}\right)\delta_p$ as a functional on an appropriate space of functions, in our case the finite-dimensional space $PL(\Sigma)$ of piecewise linear functions on Σ. What we need to know is how $\left(\frac{\partial}{\partial u} - i\frac{\partial}{\partial v}\right)\delta_p$ acts on elements of this function space.

For any function f smooth in a neighborhood of p, one has

$$\begin{aligned}\int\int_\Sigma f\left(\frac{\partial}{\partial u} - i\frac{\partial}{\partial v}\right)\delta_p dS &= -\int\int_\Sigma \left(\frac{\partial}{\partial u} - i\frac{\partial}{\partial v}\right) f\delta_p(w)dS \\ &= -\left(\frac{\partial f}{\partial u} - i\frac{\partial f}{\partial v}\right)|_p,\end{aligned}$$

and for $f \in PL(\Sigma)$, this last quantity is completely determined by the value of f at A, B, and C.

Choose the u and the v axes so that A and B are along the u axis, and the positive v axis points towards C. Then one may easily compute that

$$\begin{aligned}\frac{\partial f}{\partial u} &= \frac{f_B - f_A}{\|B - A\|}, \\ \frac{\partial f}{\partial v} &= \frac{f_C - f_D}{\|C - D\|},\end{aligned}$$

where D is the orthogonal projection of C on AB.

To calculate D, let θ be such that

$$D = A + \theta(B - A).$$

Then by the linearity of f, $f_D = f_A + \theta(f_B - f_A)$, and since $(C - D) \perp (B - A)$, we have

$$\langle C - A - \theta(B - A), B - A \rangle = 0,$$

where here and throughout this paper we use $\langle , \rangle$ to denote an inner product. Thus

$$\theta = \frac{\langle C - A, B - A \rangle}{\|B - A\|^2}.$$

If we put this all together, we have for $f \in PL(\Sigma)$,

$$\begin{aligned}
\int\int_\Sigma f \left(\frac{\partial}{\partial u} - i \frac{\partial}{\partial v} \right) \delta_p dS &= - \left(\frac{\partial f}{\partial u} - i \frac{\partial f}{\partial v} \right) |_p \\
&= - \left(\frac{f_B - f_A}{\|B - A\|} - i \frac{f_C - f_D}{\|C - D\|} \right) \\
&= \frac{f_A}{\|B - A\|} - \frac{f_B}{\|B - A\|} + i \frac{f_C - (f_A + \theta(f_B - f_A))}{\|C - D\|}
\end{aligned}$$

3.2 Finite Elements

We will now briefly outline the finite element method for finding our approximation to z. The heart of the method simply involves the solution of a system of linear equations. See [13] for details about this method.

It is a classical fact [22] that $z = x + iy$ is a minimizer of the Dirichlet functional

$$\mathbf{D}(z) := \frac{1}{2} \int\int_\Sigma \left\{ |\nabla z|^2 + 2z \left(\frac{\partial}{\partial u} - i \frac{\partial}{\partial v} \right) \delta_p \right\} dS,$$

where ∇z is the gradient with respect to the induced metric on Σ.

Equivalently, one may show that z satisfies (1) if and only if for all smooth test functions f, we have

$$\int\int_\Sigma \left\{ \nabla z \cdot \nabla f + f \left(\frac{\partial}{\partial u} - i \frac{\partial}{\partial v} \right) \delta_p \right\} dS = 0 \tag{2}$$

or

$$\int\int_\Sigma \nabla z \cdot \nabla f dS = \left(\frac{\partial f}{\partial u} - i \frac{\partial f}{\partial v} \right) |_p. \tag{3}$$

The latter formulation is the key to the finite element approximation of the solution to (1) on the triangulated surface Σ. We restrict our attention to $PL(\Sigma)$, and seek a $z \in PL(\Sigma)$ such that (3) holds for all $f \in PL(\Sigma)$.

For each vertex $P \in \Sigma$, let ϕ_P be the continuous function such that

$$\begin{array}{lcl} \phi_P(P) & = & 1, \\ \phi_P(Q) & = & 0,\ Q \neq P,\ Q \text{ a vertex}, \\ \phi_P \text{ is linear on each triangle.} & & \end{array} \tag{4}$$

Then these ϕ_P form a basis for $PL(\Sigma)$ and we seek a z of the form

$$z = \sum_{P \text{ vertex of } \Sigma} z_P \phi_P,$$

for some vector of complex constants (z_P). Further, since (3) is linear in f, it is enough to show that (3) holds whenever $f = \phi_Q$ for some Q.

In short, we want to find a vector of complex numbers $z = (z_P)$, containing one element per vertex, such that for all Q,

$$\sum_P z_P \int\int \nabla\phi_P \cdot \nabla\phi_Q dS = \frac{\partial\phi_Q}{\partial u}(p) - i\frac{\partial\phi_Q}{\partial v}(p). \tag{5}$$

3.3 Formulation in Matrix Terms

The formulation (5) is simply a system of linear equations in the complex unknowns z_P.

Accordingly, we introduce the matrix (D_{PQ}), where

$$D_{PQ} = \int\int \nabla\phi_P \cdot \nabla\phi_Q dS,$$

for each pair of vertices P, Q. It is easily seen that $D_{PQ} \neq 0$ only if P and Q are connected by some edge in the triangulation. Thus the matrix D is sparse.

Suppose PQ is an edge belonging to two triangles, PQR, and PQS. A formula from finite-element theory [13], easily verified with basic calculus, says that

$$D_{PQ} = -\frac{1}{2}\left\{\cot\angle R + \cot\angle S\right\}, \quad P \neq Q, \tag{6}$$

where $\angle R$ is the angle at the vertex R in the triangle PQR, and $\angle S$ is the angle at the vertex S in the triangle PQS. (See Figure 1.)

Since

$$\sum_P D_{PQ} = \sum_P \int \nabla\phi_P \cdot \nabla\phi_Q = \int \nabla 1 \cdot \nabla\phi_Q = 0, \tag{7}$$

we see that the diagonal elements of D may be found from

$$D_{PP} = -\sum_{P \neq Q} D_{PQ}. \tag{8}$$

Let us also introduce vectors $a = (a_Q) = (\frac{\partial\phi_Q}{\partial u}(p))$ and $b = (b_Q) = (\frac{\partial\phi_Q}{\partial v}(p))$. Then equation (5), becomes, in matrix terms,

$$Dx = a \tag{9}$$

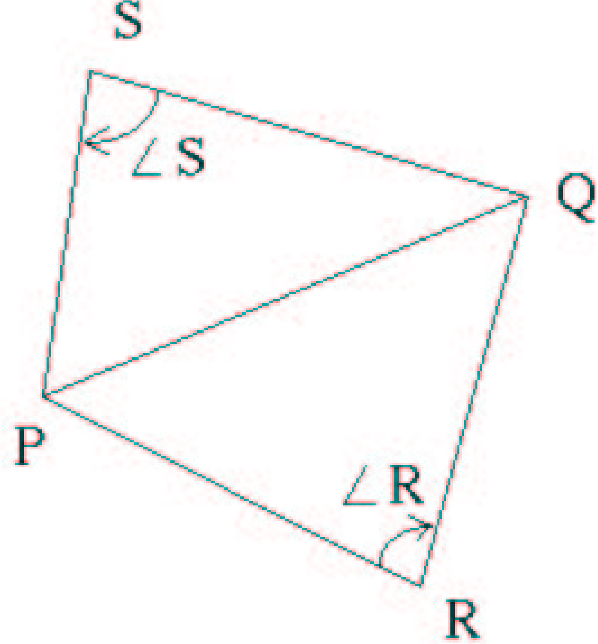

Figure 1: Triangle Geometry

$$Dy = -b \tag{10}$$

Where, using our formula for $\left(\frac{\partial}{\partial u} - i\frac{\partial}{\partial v}\right)\delta_p$ derived in Section 3.1, we have

$$a_Q - ib_Q := \begin{cases} 0 & Q \notin \{A, B, C\}, \\ \frac{-1}{||B-A||} + i\frac{1-\theta}{||C-E||} & Q = A, \\ \frac{1}{||B-A||} + i\frac{\theta}{||C-E||} & Q = B, \\ i\frac{-1}{||C-E||} & Q = C. \end{cases} \tag{11}$$

3.4 Summary of Algorithm

So we may summarize the finite element procedure for the construction of the flattening map z as follows:

(1) Compute D_{PQ}, a_Q and b_Q using the formulas (6,8,11) above.

(2) Solve the systems of linear equations (9,10) to obtain the piecewise linear harmonic functions

$$x = \sum_Q x_Q\phi_Q, \quad y = \sum_Q y_Q\phi_Q.$$

and a conformal mapping $z = x + iy$ onto the complex plane.

(3) Compose $z = x + iy$ with inverse stereographic projection to get a conformal map to the unit sphere. Specifically, send the point $x + iy$ to the point $(2x/(1 + r^2), 2y/(1 + r^2), 2r^2/(1 + r^2) - 1)$, where $r^2 = x^2 + y^2$.

4 Construction of the Flattening Map

In this section, we give methods for carrying out the finite element procedure discussed in the previous section by solving the equations (9, 10).

Note first that since $\sum_Q D_{PQ} = 0$ for all P, the matrix $D = (D_{PQ})$ is singular, and so we need to show that solutions to (9, 10) exist. In addition, we will show that D enjoys several properties which make the solution of (9, 10) easy to compute numerically.

We remark that if $Dx = 0$ for some non-zero vector $x = (x_P)$, then all the elements of x are the same. To demonstrate this, suppose $Dx = 0$. Then clearly

$$\sum_{P,Q} D_{PQ} x_P x_Q = 0. \tag{12}$$

Further, by definition of the matrix D_{PQ} we have

$$\int\int_\Sigma |\nabla u|^2 dS = \sum_{P,Q} D_{PQ} x_P x_Q \tag{13}$$

where $u \in PL(\Sigma)$ is the function with $u(Q) = x_Q$ for all vertices Q. Equations (12) and (13) together imply that u is constant, and hence that all x_Q are equal. We conclude that the kernel of D is

$$H := \{\lambda(1, 1, ..., 1)^T \mid \lambda \in \mathbf{R}\}.$$

This is similar to the result from differential geometry which says that the only harmonic functions on a compact, connected, oriented Riemannian manifold are the constant functions.

By construction, D is real, symmetric, and diagonally dominant with positive diagonal entries. This implies that D is positive semi-definite, and together with the analysis above, we see that D maps $H^\perp$, the orthogonal complement of H, bijectively to itself. Thus the equation $Dx = a$ is solvable if and only if $a \in H^\perp$, i.e., if $\sum_P a_P = 0$, and this solution is unique up to addition of an element of H. We note that the right-hand sides of (9, 10) are indeed in $H^\perp$.

Since D, restricted to $H^\perp$, is symmetric and positive definite, equations (9, 10) are particularly well suited for numerical solution by methods such as the conjugate gradient method. Although D is singular, this method involves only multiplications by D and addition of vectors in $H^\perp$, and so quite literally solves the equations for D restricted to $H^\perp$.

If one prefers, alternative methods to solving the system of equations can be used to avoid working directly with the entire singular matrix D. This may be of use if one wishes to use a linear algebra package which was not designed to handle such singular matrices. We present one such method here for completeness; we have found that this method and the one mentioned above are equally effective. On the triangulated surface Σ, choose a triangle ABC. Choose an arbitrary triangle $(A', B', C') \subset \mathbf{C}$, and solve

$$\sum_Q D_{PQ} \tilde{z}_Q = 0, \tag{14}$$

$$\tilde{z}_A = A', \ \tilde{z}_B = B', \ \tilde{z}_C = C'.$$

for the unknowns $\tilde{z}_P, P \notin \{A, B, C\}$.

Next, for $P \in \{A, B, C\}$, set

$$\tilde{a}_P + i\tilde{b}_P := \sum_Q D_{PQ}\tilde{z}_Q.$$

If $P \notin \{A, B, C\}$, we set

$$\tilde{a}_P + i\tilde{b}_P := 0$$

so that the computed $\{\tilde{z}_Q\}$ is a solution of

$$\sum_Q D_{PQ}\tilde{z}_Q = \tilde{a}_P + i\tilde{b}_P.$$

Note that this, together with (7) gives

$$\sum_P \tilde{a}_P + i\tilde{b}_P = \sum_P \sum_Q D_{PQ}\tilde{z}_Q = \sum_Q \left(\tilde{z}_Q \sum_P D_{PQ}\right) = 0. \tag{15}$$

We now make the key observation that the space of vectors

$$\{(f_P) : f_Q = 0, Q \notin \{A, B, C\}, \sum_P f_P = 0\}$$

is two-dimensional. It is easy to show that $(\tilde{a}_P)$ and $(\tilde{b}_P)$ span this space and that the space also contains (a_P) and (b_p) as defined by (11). Thus (a_P) and (b_P) must be linear combinations of $(\tilde{a}_P)$ and $(\tilde{b}_P)$. Hence, we can solve for $\alpha, \beta, \gamma, \delta$ such that

$$\begin{aligned} a_P &= \alpha\tilde{a}_P + \beta\tilde{b}_P, \quad \forall P \in \Sigma, \\ b_P &= \gamma\tilde{a}_P + \delta\tilde{b}_P, \quad \forall P \in \Sigma. \end{aligned} \tag{16}$$

We write

$$\tilde{z}_P := \tilde{x}_P + i\tilde{y}_P,$$

and then the solutions x_P and y_P to equations (9, 10) are given by

$$x_P = \alpha\tilde{x}_P + \beta\tilde{y}_P, \quad \forall P \in \Sigma \tag{17}$$
$$y_P = \gamma\tilde{x}_P + \delta\tilde{y}_P, \quad \forall P \in \Sigma. \tag{18}$$

We therefore have the following algorithm for computing z_P:

(1) Solve the system of equations (14).

(2) Find the constants $\alpha, \beta, \gamma, \delta$ from (16).

(3) Calculate x_P and y_P from (17, 18). Set $z_P = x_P + iy_P$.

5 Brief Review of 3D Segmentation

In this section, we very briefly review some previous work on segmentation according to weighted mean curvature flows as described in [5, 15, 25]. We follow the treatment of [15] here.

5.1 Mean Curvature Surface Evolution

The key to the segmentation approach is a modification of the ordinary area functional, and the corresponding gradient flow. In order to motivate this, we need to briefly summarize some of the literature on mean curvature motion and the resulting theory of minimal surfaces. For all the key concepts in differential geometry, we refer the reader to [9].

Let $S : [0,1] \times [0,1] \to \mathbf{R}^3$ denote a compact embedded surface with (local) coordinates (u, v). Let H denote the mean curvature, that is, H is the arithmetic mean of the principal curvatures. (Recall that at each point p the surface S has two *principal curvatures* given by the maximum and minimum curvatures of planar curves which are cut out on the surface by planes meeting the surface orthogonally at p.) We let $\mathbf{N}$ denote the inward unit normal. Set

$$S_u := \frac{\partial S}{\partial u}, \quad S_v := \frac{\partial S}{\partial v}.$$

Then the infinitesimal area on S is given by

$$dS = (\|S_u\|^2\|S_v\|^2 - \langle S_u, S_v\rangle^2)^{1/2} du\, dv.$$

We make use of the fact that the gradient flow associated to the area functional for surfaces can be defined in terms of the mean curvature. (See [18] and the references therein.) More precisely, for a family of surfaces $S = S(u, v, t)$ depending on a parameter t, consider the area functional

$$A(t) := \int_0^1 \int_0^1 (\|S_u\|^2\|S_v\|^2 - \langle S_u, S_v\rangle^2)^{1/2} du\, dv.$$

Taking the first variation, and using integration by parts, it is easy to compute that

$$\frac{dA}{dt} = -\int\int_S \langle \frac{\partial S}{\partial t}, H\mathbf{N}\rangle dS.$$

Therefore the direction in which the area is shrinking most rapidly (using only local information) is given by

$$\frac{\partial S}{\partial t} = H\mathbf{N}. \tag{19}$$

Consequently, this flow is very closely connected to the theory of minimal surfaces (surfaces of minimal area with given boundary conditions).

5.2 3-D Active Contour Models

We can now formulate our geometric 3-D contour models based on the mean surface motion. Our method is derived by modifying the Euclidean area by a function which depends on the salient image features which we wish to capture.

Indeed, let $\phi : \Omega \to \mathbf{R}$ be a positive differentiable function defined on some open subset of $\mathbf{R}^3$. The function $\phi(x, y, z)$ will play the role of a "stopping" function. Thus the function $\phi(x, y, z)$ will depend on the given grey-level image. Explicitly, the term $\phi(x, y, z)$ may chosen to be small near a 3D edge, and so acts to stop the evolution when the 3D contour reaches the edge. For example, as in the 2D case, we can choose

$$\phi := \frac{1}{1 + \|\nabla G_\sigma * I\|^2}, \tag{20}$$

where $I = I(x, y, z)$ is the (grey-scale) volumetric image and G_σ is a Gaussian (smoothing) filter.

What we propose to do is to replace the Euclidean area given above by a modified (conformal) area depending on ϕ namely,

$$dS_\phi := \phi dS.$$

Indeed, for a family of surfaces (with parameter t), consider the ϕ-area functional

$$A_\phi(t) := \int\int_S dS_\phi.$$

Taking the first variation and using a simple integration by parts argument we get that

$$\frac{dA_\phi}{dt} = -\int\int_S \langle \frac{\partial S}{\partial t}, (\phi H - \nabla\phi \cdot \mathbf{N})\mathbf{N} \rangle dS.$$

The corresponding gradient flow is then

$$\frac{\partial S}{\partial t} = (\phi H - \nabla\phi \cdot \mathbf{N})\mathbf{N}. \tag{21}$$

Notice that Euclidean conformal area dS_ϕ is small near an edge. Thus we would expect and initial 3D contour to flow to the potential well indicated by the evolution (21). A method for implementing a curvature driven flow such as that given by (21) is based on level sets in which the evolving surface is embedded as the zero level set of the graph of a function; see [19, 20, 21] for full details about this. This technique has the advantage of automatically taking into account topological changes in the evolving surface (splitting and merging), and so has been very useful in snake based segmentation approaches such as the one we are using here. (For the cortical surface which has the topology of the sphere no breaking or merging is of course necessary.)

The level set version of (21) [19, 20, 21] is given in terms of the evolving function $\Psi(x, y, z, t)$ by

$$\frac{\partial \Psi}{\partial t} = \phi \|\nabla\Psi\| \mathrm{div}(\frac{\nabla\Psi}{\|\nabla\Psi\|}) + \nabla\phi \cdot \nabla\Psi. \tag{22}$$

A constant inflation term ν may be added to give the model

$$\Psi_t = \phi \|\nabla\Psi\| (\mathrm{div}(\frac{\nabla\Psi}{\|\nabla\Psi\|}) + \nu) + \nabla\phi \cdot \nabla\Psi. \tag{23}$$

This inflationary constant may be taken to be either positive (inward evolution) or negative in which case it would have an outward or expanding effect. For the level set implementation, we take Ψ to be negative in the interior and positive in the exterior of the zero level set.

6 Experimental Results

We tested our algorithm by flattening the brain surface contained in a $256 \times 256 \times 124$ MR brain image provided by the Surgical Planning Laboratory of Brigham and Women's Hospital in Boston. Three slices of the original data set are given in Figure 2. These consist of sagittal T1 weighted gradient echo images of a patient with a brain tumor. The three images progress from a close to midline slice to a lateral slice. We chose a brain with a tumor to illustrate the effect of the flattening on both normal and pathological features in an MR brain set.

First, using the segmentation algorithm described in the previous section, we found the brain cortical surface, i.e the gray matter/CSF interface. Unfortunately, the segmentation algorithm itself does not guarantee that the surface found will be of genus zero. In fact, it may contain numerous minute handles which arise because the boundary between the cortical surface and the surrounding fluid, as represented in the data set, may not be sharp. We have used a morphological based method by which these handles can be effectively removed and a surface of genus zero extracted. This is done in such a way that the large-scale geometry of the surface is not badly affected.

The VTK Toolkit [23] was used to obtain a triangularization of the surface, which we proceeded to smooth slightly to reduce the effects of aliasing. This was done by using the flow according to mean curvature. This also allowed us to obtain a measure of the convexity and concavity of points on the brain surface by considering the mean curvature vector.

Once the surface was smoothed, we used the method described in the previous sections to find a flattening map to the plane and then composed this map with a map from the plane to the unit sphere using inverse stereographic projection described at the end of Section 3.4. This composition gives us a bijective conformal map from the surface to the sphere.

Note that it is not practical to view the planar mapping directly in its entirety, because stereographic projection stretches areas near the north pole too much to be useful. In fact it is not possible to map a sphere, a nearly complete sphere, or any other similarly shaped surface to the plane in any way without major distortion. However, smaller surface patches may be mapped to the plane with a more reasonable amount of distortion, and in fact the "best" (in terms of length distortion) mapping to the plane from a sphere with a geodesic disk removed is known. For an accessible treatment of some of the relevant mathematics and results, see [17]. In practice, we have not found the distortion of area near the north pole to be a problem in solving the linear equations for our flattening map. The method seems to be stable across a wide variety of surface shapes and varying fineness of triangulations.

After flattening the brain surface, we used mean curvature to color corresponding points on the two surfaces (the lighter the point the higher the mean curvature on the brain surface). This provided us with an effective way to see how the flattening process acted on the gyral lines of the brain surface. This is shown in Figures 3 and 4, which provide several views of the cortical surface and the corresponding areas on the sphere. Note the tumor on the right parietal lobe visible in the vertex view. It is interesting to see how the conformality of the mapping from the brain surface to the sphere results in a flattened image which is locally very similar in appearance to the original.

Next, we tested our process on the more highly convoluted surface which is defined by the boundary between the white and gray matter within the brain. To extract this boundary, we used a combination of the method based on smoothing posterior probabilities as described in [27], and the segmentation method described in the previous section. (See also [14, 29, 30, 31], and the references therein for other approaches to brain segmentation.) Once the surface was obtained, our flattening method was applied exactly as it was for the cortical surface. The result of this process is shown in Figure 5. Note that much of the white matter surface is hidden within its deep convolutions, but that such areas on the sphere are clearly visible.

One of the advantages of the flattening method we are presenting is its speed. The white matter surface shown in Figure 5 is composed of 430,000 triangular faces, yet the flattening procedure took less than 6 minutes using a Sun Ultrasparc 10. For surfaces with triangles in the tens of thousands, the flattening procedure takes only a few seconds. This is primarily due to the fact that the heart of our procedure involves only the solution of two sparse systems of linear equations.

6.1 Some Quantitative Measurements

By definition, a conformal mapping is one which preserves angles. To test the effectiveness of our procedure in producing such a map, we computed statistics which reflected how closely surface angles were preserved. The sum of the angles around any vertex in our flattened planar representation of the surface is of course 360 degrees. In fact, if any smooth surface is tessellated with curvilinear triangles, then the sum of the surface angles around any vertex will also be 360 degrees. This can be seen at the north pole on the globe, the angles being those formed by the meridians. However, this is not true on a triangulated surface. In fact, the sum of the angles of triangles around a vertex will be greater than or less than 360 degrees depending on whether the surface has negative or positive Gaussian curvature at the vertex respectively. This effect is particularly noticeable for the surfaces we obtained from MRI data where aliasing caused many sharp corners to appear at the voxel level. Hence we found it necessary to compute statistics for synthetic surfaces on which we could obtain more accurate angular measurements. An example of such a surface, containing 8704 triangles, is presented in Figure 6. We found that the standard deviation of the differences between angles on this surface and its flattened representation was under 4 degrees. Deviations of this order were typical for the various surfaces we tested.

It is generally not possible to map a surface with non-constant Gaussian curvature to the plane or sphere in a way which preserves both angles and areas. However, a conformal mapping, being a "similarity in the small," acts on small areas essentially by scaling them by some factor. This scaling factor will vary over different parts of the surface, and naturally this variance will tend to be larger over larger areas. Further, we have found that the scaling factor tends to vary most over regions which contain large variances in the Gaussian curvature. Again, we used a synthetic surface to calculate some statistics describing this variance; the "noisy" surface we extracted from the MRI data being highly convoluted even across areas representing 0.2 percent of the surface area. For the synthetic surface shown in Figure 6, we randomly selected 50 surface patches, each representing roughly one tenth of the original surface. We scaled each patch and its spherical counterpart so that the mean area of their triangles was one. We then calculated the standard deviation of the difference in area between corresponding triangles. This value ranged from 0.26 to 0.70, with an average value of 0.44.

7 Conclusions

In this paper, we described a general method based on a discretization of the Laplace-Beltrami operator for flattening a surface in a manner which preserves the local geometry. The approach can be carried out using a finite element method which takes into account the special boundary conditions. We also illustrated the technique on the brain surface and white matter of an MR brain data set.

In addition to the functional MRI mentioned at the beginning of this paper we have several other applications in mind. We point out that inverting the flattening map allows us easily to establish orthogonal coordinates on the surface. Further, the method allows us to find north and south poles on a highly convoluted surface such as the brain, giving an alternative method to that discussed in [3].

As is well-known, a number of pathologies have been associated with deformations of brain structures. We are very hopeful that these techniques will be useful in quantitatively describing such pathologies. Finally, the conformal technique may also be utilized for automatic texture mapping.

One of the benefits of using conformal mappings of this type is that the mathematical theory predicts that such bijective, angle preserving mappings exist, in contrast to isometric mappings. If a quasi-length or area preserving mapping is desired, we believe that the conformal mapping technique is a very reasonable starting point, since it effectively "unfolds" the surface, preserving local geometry, and avoiding the problem of non-bijectivity from triangle "flipping" which can occur with some other approaches. The basic idea is that it seems to be easier to maintain bijectivity while minimizing length or area distortion than it is to produce bijectivity and minimal distortion simultaneously.

In particular, we can establish smooth families of vector fields on the sphere and move points around according to the flow of these fields to minimize certain distortions. This amounts to solving an ordinary differential equation on the sphere. One such family of vector fields, one which corrects for area distortion, is being considered in some very recent work [2]. By running the flow for different periods of time we can compromise between conformality and area preservation. Another flow with which we are working is one which is divergence free, and thus area preserving, while at the same time flows in a direction which decreases the standard energy functional for mappings between surfaces and thereby decreases angular distortion. We hope to use these flows in combination, and report on the results soon.

We are planning on exploring these and other avenues in our future research.

8 Mathematical Appendix

In this section, we outline the derivation the partial differential equation (1). See also [1, 11, 22] and the references therein.

We first choose conformal coordinates (u, v) on Σ near p, with $u = v = 0$ at p. (Conformal coordinates u, v are such that the metric at the point p is of the form $ds^2 = \lambda^2(p)(du^2 + dv^2)$. We can always insure that at the particular point p, $\lambda(p) = 1$. One can show that such conformal coordinates always exist [10].)

Put $w = u + iv$. Since z is one to one, it follows that it has a simple pole at p, and thus a Laurent series expansion given by

$$z(w) = \frac{A}{w} + B + Cw + Dw^2 \cdots .$$

Since all terms except the first in this Laurent series are smooth (harmonic) at $w = 0$, applying Δ to both sides yields

$$\Delta z = A\Delta\left(\frac{1}{w}\right).$$

We need only find z up to a constant multiple, so taking $A = \frac{1}{2\pi}$,

$$\begin{aligned}
\Delta z = \frac{1}{2\pi}\Delta\left(\frac{1}{w}\right) &= \frac{1}{2\pi}\Delta\left(\frac{\partial}{\partial u} - i\frac{\partial}{\partial v}\right)\log|w| \\
&= \frac{1}{2\pi}\left(\frac{\partial}{\partial u} - i\frac{\partial}{\partial v}\right)\Delta\log|w| \\
&= \frac{1}{2\pi}\left(\frac{\partial}{\partial u} - i\frac{\partial}{\partial v}\right)(2\pi\delta_p(w)) \\
&= \left(\frac{\partial}{\partial u} - i\frac{\partial}{\partial v}\right)\delta_p(w),
\end{aligned}$$

where we have used the fact that $\frac{1}{2\pi}\log|w|$ is the fundamental solution for the operator Δ. Since $1/w \in L_{1,loc}(\mathbf{C})$, i.e. is locally integrable, this computation is also valid in the distributional sense, i.e. in the space of distributions $\mathcal{D}'(\mathbf{C})$ [22].

We may now prove the following:

Theorem 1 *The conformal map* $z_0 : \Sigma\backslash\{p\} \to S^2\backslash\{\textit{north pole}\} \cong \mathbf{C}$ *may be obtained by solving the equation*

$$\Delta z = \left(\frac{\partial}{\partial u} - i\frac{\partial}{\partial v}\right)\delta_p. \tag{24}$$

Proof. From the above argument, we need only prove existence. But finding a solution of (24) is possible (see [22]) because the right-hand side integrates out to zero:

$$\int\int_\Sigma \left(\frac{\partial}{\partial u} - i\frac{\partial}{\partial v}\right)\delta_p dS = -\left(\frac{\partial}{\partial u} - i\frac{\partial}{\partial v}\right)(1)|_p = 0,$$

in direct analogy to our discussion on the solvability of $Dx = a$. $\square$

References

[1] S. Angenent, S. Haker, A. Tannenbaum, and R. Kikinis, "Conformal maps and flattening the brain surface," Technical Report, Department of Electrical and Computer Engineering, University of Minnesota, January 1998.

[2] S. Angenent, S. Haker, A. Tannenbaum, and R. Kikinis, "On area preserving mappings of surfaces with minimal distortion," in prepartion.

[3] C. Brechbühler, G. Gerig, and O. Kübler, "Parametrization of closed surfaces for 3D shape description," Technical Report, Communication Technology Laboratory, ETH, Zürich, Switzerland, 1996.

[4] G. J. Carman, H. A. Drury, and D. C. Van Essen, "Computational methods for reconstructing and unfolding the cerebral cortex," *Cereb. Cortex*, **5(6)**, (1995), pp. 506-517.

[5] V. Caselles, R. Kimmel, and G. Sapiro, , "Geodesic snakes," *Int. Journal of Computer Vision*, 1997.

[6] A. Dale and M. Sereno, "Improved localization of cortical activity by combining EEG and MEG with MRI cortical surface reconstruction: a linear approach," *Journal of Cognitive Neuroscience* **5** (1993), pp. 162-176.

[7] C. Davatzikos and R. N. Bryan, "Using a deformable surface model to obtain a shape representation of the cortex," *IEEE Transactions on Medical Imaging,* **15**, (1996), pp. 785-795.

[8] H. Drury, D. van Essen, C. Anderson, C. Lee, T. Coogan, and J. Lewis, "Computerized mappings of the cerebral cortex: a multiresolution flattening method and a surface-based coordinate system," *Journal of Cognitive Neuroscience* **8** (1996), pp. 1-28.

[9] M. P. Do Carmo, *Differential Geometry of Curves and Surfaces*, Prentice-Hall, Inc., New Jersey, 1976.

[10] M. P. Do Carmo, *Riemannian Geometry*, Prentice-Hall, Inc. New Jersey, 1992.

[11] H. Farkas and I. Kra, *Riemann Surfaces*, Springer-Verlag, New York 1991.

[12] I. Hollander, "Cerebral cartography - A method for visualizing cortical structures," *Computerized Medical Imaging and Graphics,* **19**, (1995), pp. 397-415.

[13] T. Hughes, *The Finite Element Method,* Prentice-Hall, New Jersey, 1987.

[14] T. Kapur, W. Grimson, W. Wells III, and R. Kikinis, "Segmentation of brain tissue from magnetic resonance images," *Medical Image Analysis* **1** (1996), pp. 109-127.

[15] S. Kichenasamy, A. Kumar, P. Olver, A. Tannenbaum, A. Yezzi, "Conformal curvature flows: from phase transitions to active contours," *Archive Rational Mechanics and Analysis* **134** (1996), pp. 275-301.

[16] D. MacDonald, D. D. Avis, A. C. and Evans, "Multiple surface identification and matching in magnetic resonance images," in *Visualization in Biomedical Computing,* edited by R. Robb, SPIE Publications, vol. 2359, 1994, pp. 160-169.

[17] J. Milnor, "A problem in cartography," *Amer. Math. Monthly* **(76)**, (December, 1969), pp. 1101-1112.

[18] F. Morgan, *Riemannian Geometry,* John and Bartlett Publishers, Boston, 1993.

[19] S. Osher, "Riemann solvers, the entropy condition, and difference approximations," *SIAM J. Numer. Anal.* **21**, pp. 217-235, 1984.

[20] S. J. Osher and J. A. Sethian, "Fronts propagation with curvature dependent speed: Algorithms based on Hamilton-Jacobi formulations," *Journal of Computational Physics* **79**, pp. 12-49, 1988.

[21] J. A. Sethian, "A review of recent numerical algorithms for hypersurfaces moving with curvature dependent speed," *J. Differential Geometry* **31**, pp. 131-161, 1989.

[22] J. Rauch, *Partial Differential Equations*, Springer-Verlag, New York 1991.

[23] W. Schroeder, H. Martin, B. Lorensen, *The Visualization Toolkit*, Prentice-Hall, New Jersey, 1996.

[24] E. Schwartz, A. Shaw, E. Wolfson, "A Numerical solution to the generalized mapmaker's problem: Flattening nonconvex polyhedral surfaces," *IEEE Trans. Pat. Anal. Machine Intel.* **11:9** (1989), pp. 1005-1008.

[25] K. Siddiqi, A. Tannenbaum, and S. Zucker, "Area and length minimizing flows for image segmentation," *IEEE Trans. Image Processing* **7** (1998), pp. 433-444.

[26] A. Tannenbaum, "Three snippets of curve evolution theory in computer vision," *Journal of Mathematical and Computer Modelling* **24** (1996), pp. 103-119.

[27] P. Teo, G. Sapiro, and B. A. Wandell, "Creating connected representations of cortical gray matter for functional MRI visualization," to appear in *IEEE Transactions on Medical Imaging.*

[28] B. Wandell, S. Engel, and H. Hel-Or, "Creating images of the flattened cortical sheet," *Invest. Opth. and Vis. Sci.* **36** (S612), 1996.

[29] C. Xu, D. Pham, and J. Prince, "Reconstruction of the central layer of the human cerebral cortex from MR images," *Medical Image Computing and Computer-Assisted Intervention*, Springer-Verlag, pp. 481-488, 1998.

[30] X. Zeng, L. Staib, R. Schultz, and J. Duncan, "Volumetric layer segmentation using coupled surfaces propagation," *Computer Vision and Pattern Recognition*, pp. 708-715, 1998.

[31] X. Zeng, L. H. Staib, R. T. Schultz, and J. S. Duncan, "Segmentation and measurement of the cortex from 3D MR images," *Medical Image Computing and Computer-Assisted Intervention*, Springer-Verlag, pp. 519-530, 1998.

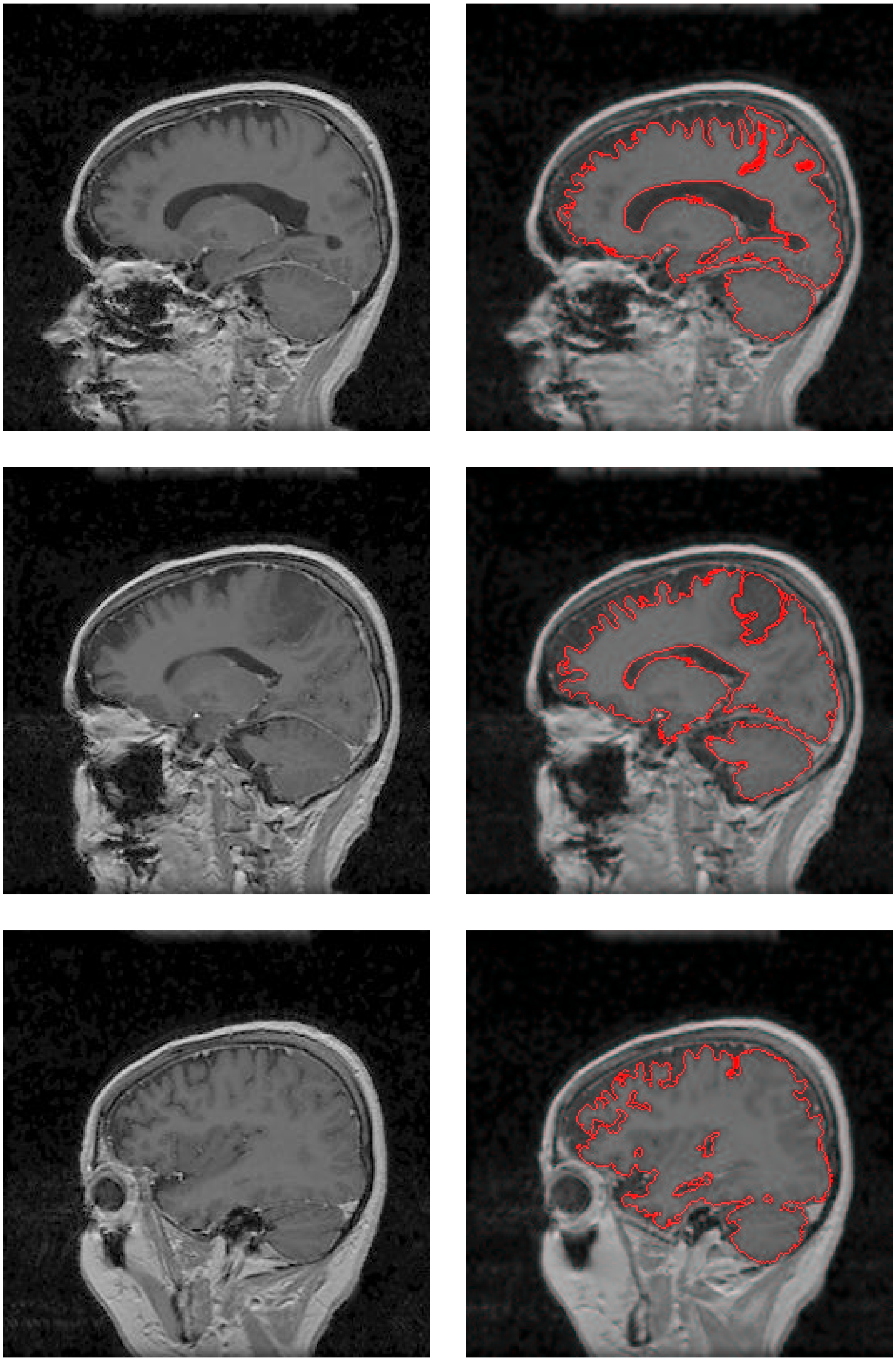

Figure 2: Three Slices of MR Brain Image with Segmentations

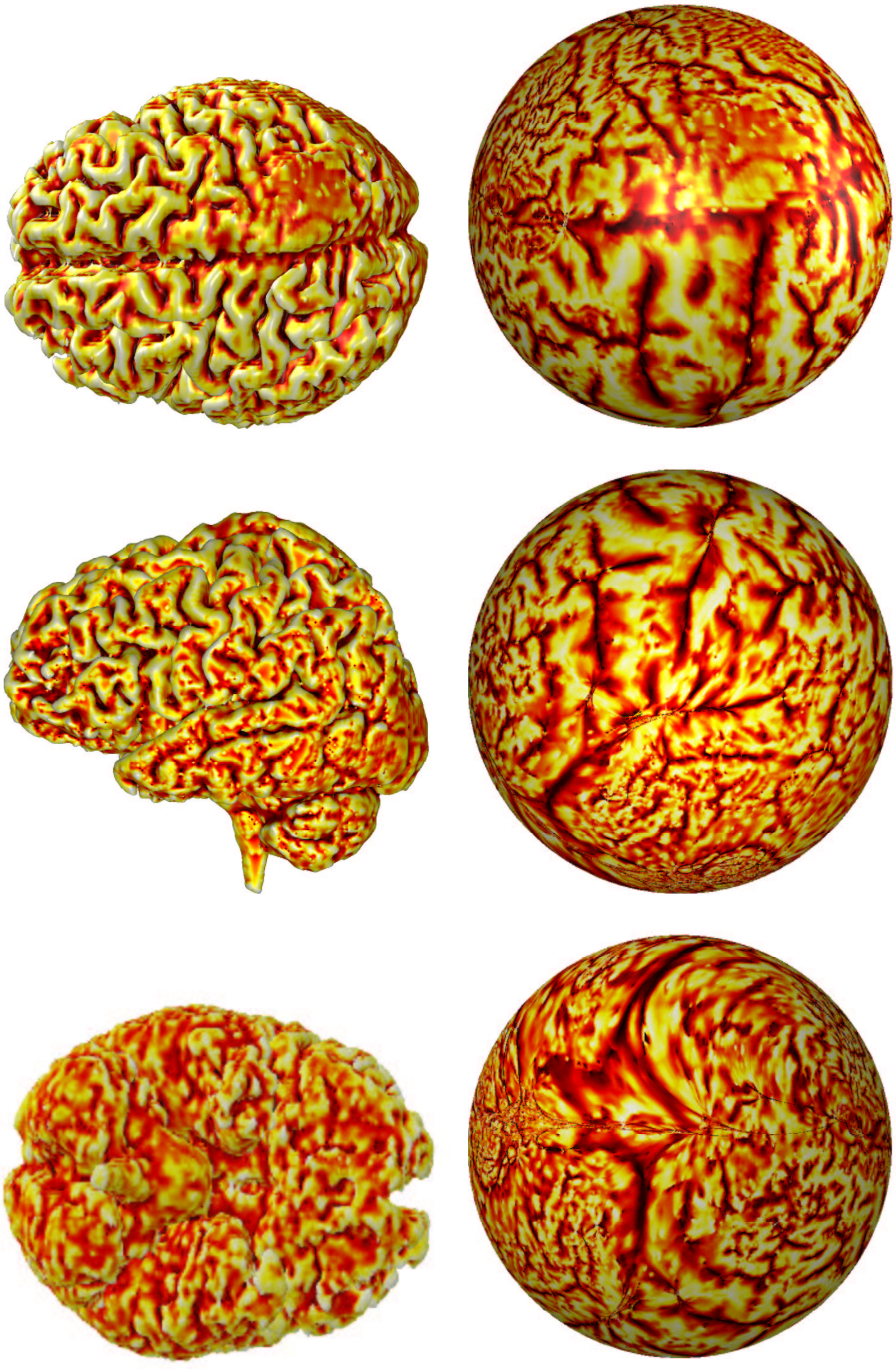

Figure 3: Three Views of the Flattened Brain Surface

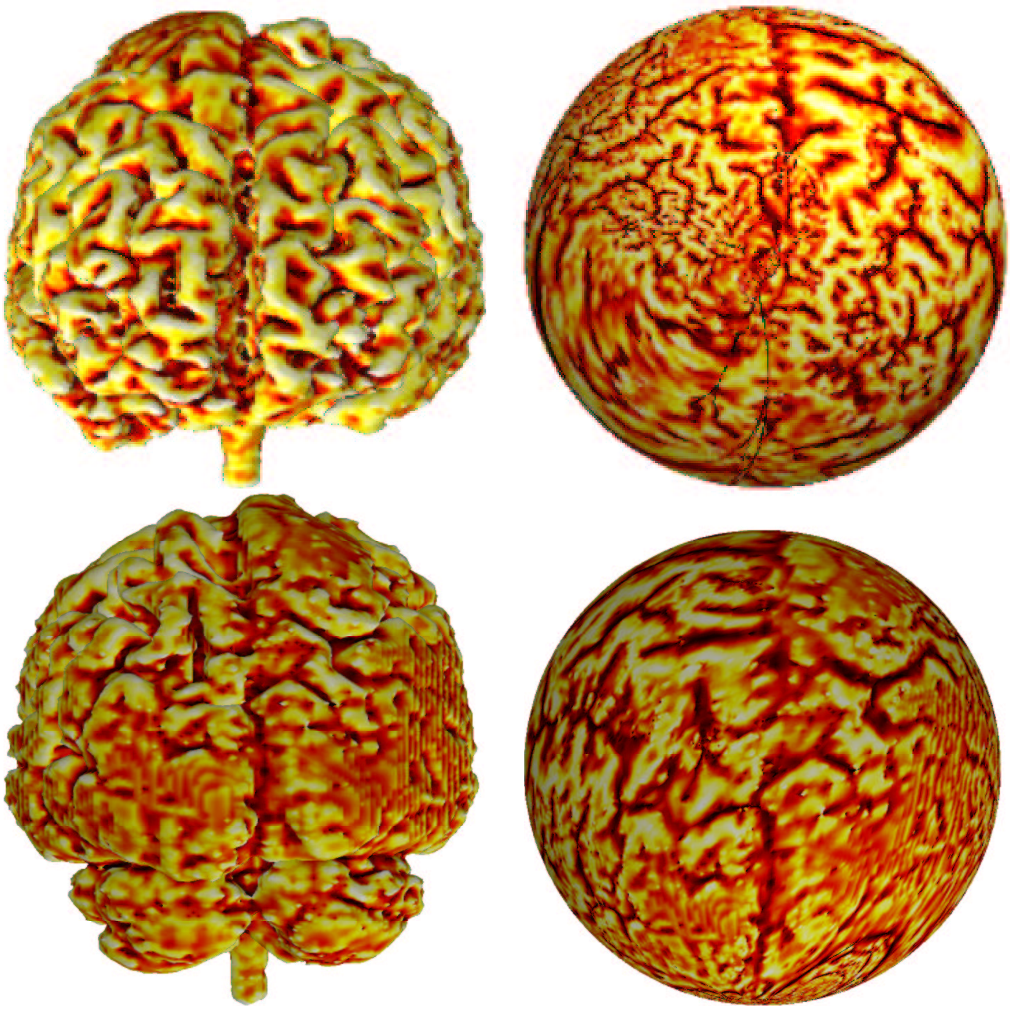

Figure 4: Two More Views of the Flattened Brain Surface

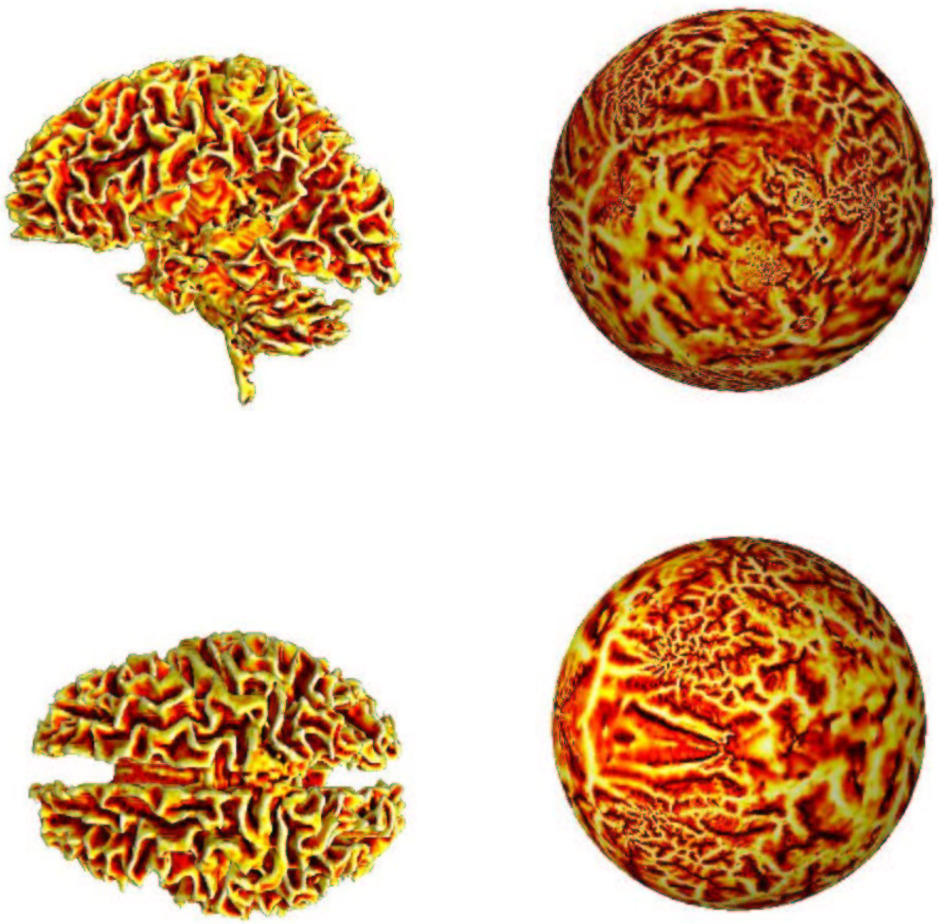

Figure 5: Two Views of the Flattened White Matter

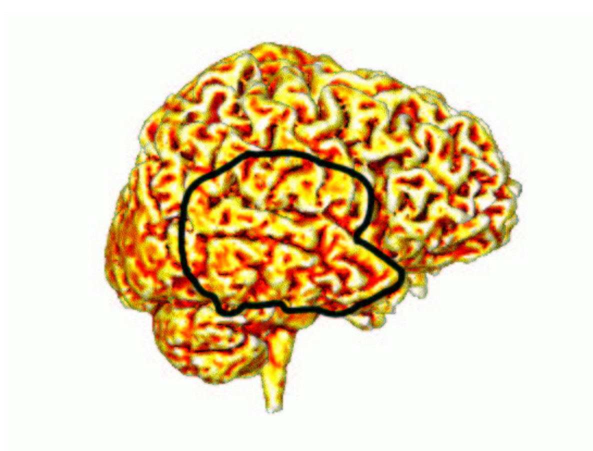

Figure 6: Outline of Flattened Region